



ISTITUTO NAZIONALE DI FISICA NUCLEARE

Sezione di Padova

INFN/AE-02/01

28 Giugno 2002

HARP Note 02-001

June 27, 2002

The HARP TOF-WALL counter construction and test

G. Barichello, F. Bobisut, A. De Min, D. Gibin, A. Guglielmi, M. Laveder, A. Menegolli,
M. Mezzetto and A. Pepato

Dipartimento di Fisica "G.Galilei" and INFN, Padova, Italy

M. Bonesini, M. Paganoni, F. Paleari and A. Tonazzo

Dipartimento di Fisica "G.Occhialini" and INFN, Milano, Italy

Abstract

In this note the preparation of the TOF-WALL scintillation counters for the PS214 experiment (HARP) at CERN PS and the laboratory tests with cosmic rays are reported. The measurement of detection efficiencies, time resolutions and attenuation of signals along the counters shows very good performances. The intrinsic time resolution resulted to be ~ 150 ps.

PACS:25.40;25.80;29.40.Mc

*Published by SIS-Pubblicazioni
Laboratori Nazionali di Frascati*

1 Introduction

The HARP experiment[1], in operation at CERN PS, was designed to measure with high precision the secondary hadrons production on various nuclear targets by proton and pion beams in the $2 \div 15$ GeV/c momentum range:

- to acquire adequate knowledge of π yields, for an optimal design of a neutrino factory where pure neutrino beams are produced by the muon decay;
- to improve substantially the calculation of the atmospheric ν flux, needed for a refined study of atmospheric ν .

The experimental exploitation requires: P measurements in the 100 MeV/c \div 10 GeV/c range, a large acceptance (also in the backward direction) and a good e, μ, π, K, p recognition. Different techniques to particle identification are used in HARP. In particular the TOF-WALL scintillation counters, 6.5×2.5 m² active area placed at 10 m of distance from the production target, allows to separate pions from kaons and protons at low momenta from a precise time of flight measurements.

2 Description of the HARP TOF-WALL counters

The TOF-WALL detector consists of 42 plastic scintillators BC-408 by Bicron [2] of length of 250 cm (28 counters), 180 cm (13 counters) and 300 cm (1 counter). The width and the thickness are 21 cm and 2.5 cm, respectively. At the two ends of each slab, plexiglass fish-tail light guides have been glued, tapered from the dimensions of the ends of the slabs to those of a plexiglass cylinder ("collar") coupled to the photocatode of a PM tube (Philips XP2020 [3]) through a disc of elastomeric material (see fig.1). The counters are wrapped in aluminium and sealed with black plastic. At the center of each counter a small quartz prism attached to a multimode CERAM OPTEC 100/110 fiber (1 m long and 100 μ m thick) [4] allows the injection of laser light pulses to control the stability of counters and electronics.

The photocatode of the PM tubes is made of $SbKCs$, a material with a low ionization potential, that allows the extraction of electrons from photons of energy $h\nu \sim 3$ eV. Quantum efficiency, $\sim 26\%$ at 401 nm, is well matched with the range of wavelengths emitted by BC-408 (see fig.2 and fig.3). The photoelectron multiplication chain consists of 1+12 $Cu-Be$ dynodes. The XP2020 is characterized by a fast rise time (~ 2 ns) and good linearity of response and it can achieve a gain G of $3 \cdot 10^7$ at typical voltage of 2200 V with a low background noise. The phototube is shielded from the magnetic fields by a cylindrical

screen of μ -metal. The time jitter of XP2020 is about 250 ps, a value among the lowest for PMT's with a 2.55 inch cathode diameter.

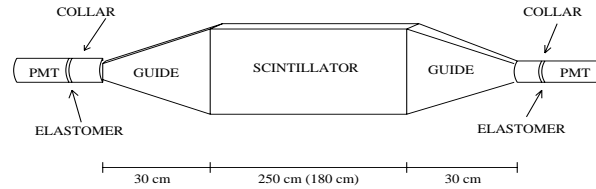


Figure 1: Coupling of the HARP scintillation counters to the PMT's through a fish tail light guide.

3 Cosmic ray test setup

The TOF-WALL scintillation counter performances were measured in laboratory with cosmic rays. The experimental set up used for the tests is shown in fig.4: five telescopes, to trigger on cosmic rays, each made of three small scintillation counters (about $10 \times 10 \text{ cm}^2$), were built to test simultaneously three TOF-WALL counters. The OR of the discriminated signals of the five telescope counters (see fig.5) gave the common start for the time measurement (CAMAC TDC mod. 2228A, 8 channels, 50 ps/count) and the 120 ns gate for the charge measurement (CAMAC ADC mod. 2249A, 10 bit, Dynamic Range, 0.25 pC/count).

Signals from the counters under test were split by a resistive partitor (see fig.6): 75% of the signal was sent to a discriminator (LECROY mod. 4413, $V_{th} = 40 \text{ mV}$), was properly delayed and then sent to a TDC individual stop. The remaining 25% was delayed and sent to an ADC, which measures integral charge in the 120 ns gate.

The CAMAC bus was connected to a VME bus through an interface put in a VME crate. Data acquisition was provided by a Bit-3 618 interface connected to a PCI board on PC through an optical link (see fig.7).

Every counter was initially tested for light tightness. A preliminary test with low statistics allowed to choose the best values of the high voltage V for the following measurements, whose aim was the study of the time resolution.

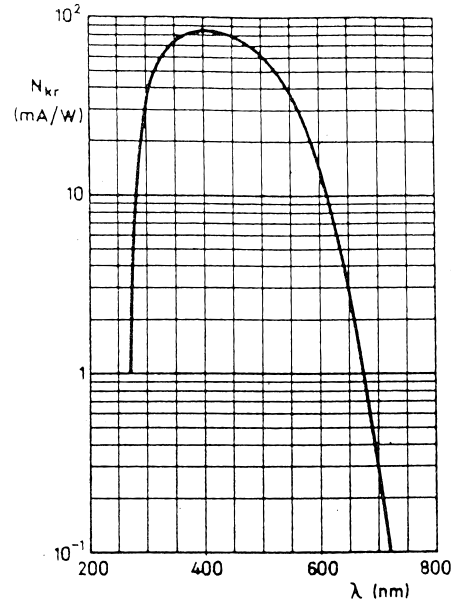


Figure 2: Spectral sensitivity of Philips XP2020 PMT.

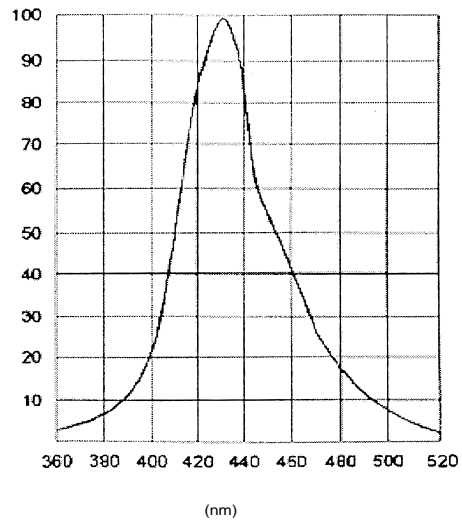
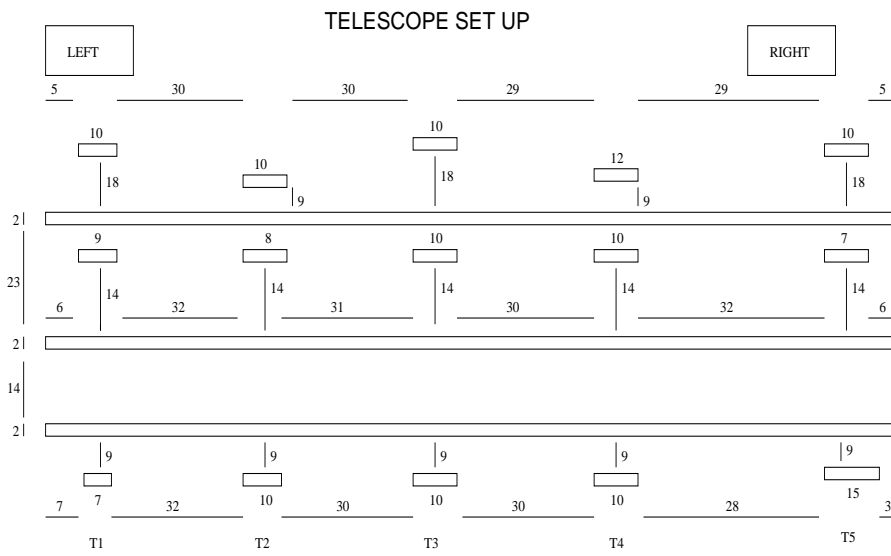
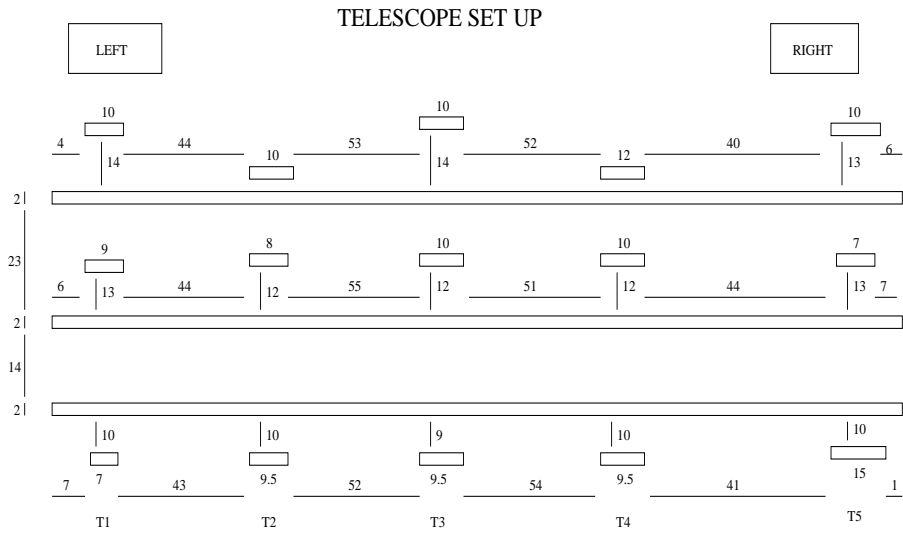


Figure 3: Emission spectrum of the BC-408 scintillator.



The distances have a precision of ~ 1 cm .

Figure 4: Geometry of the test setup for longer ($L = 250$ cm, top) and shorter ($L = 180$ cm, bottom) counters.

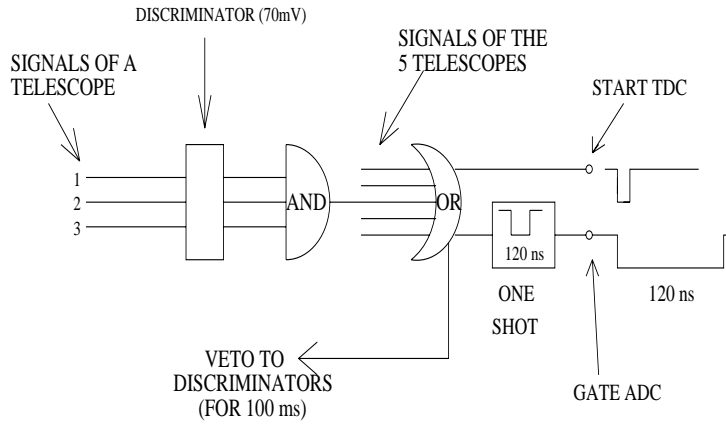


Figure 5: Block diagram of the electronics for the acquisition of telescope signals. The discriminator was a LECROY mod. 4413 (16 channels) with the threshold set at 70 mV.

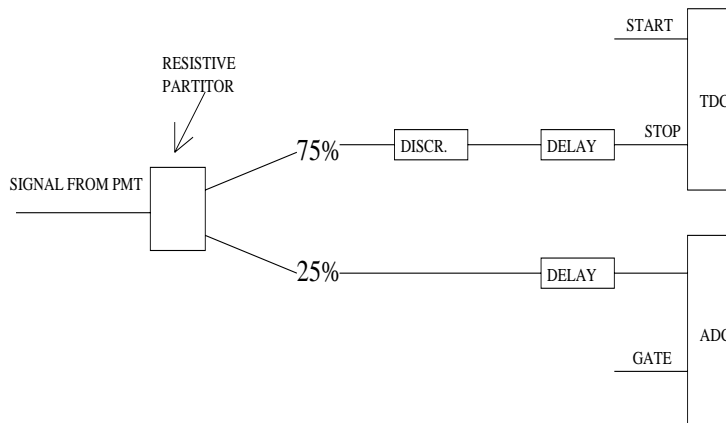


Figure 6: Block diagram showing the processing and conversion of PMT signals.

4 Analysis of cosmic ray test data

Data taken during cosmic rays tests were selected for the analysis by rejecting:

- events associated to electromagnetic showers, with more than one telescope hit along the same counter and/or charge going to full scale ADC on both PMT's of a counter;
- a few events in which none of the two PMT's connected to the same counter gave signal, indicating the presence of spurious coincidences in the telescopes.

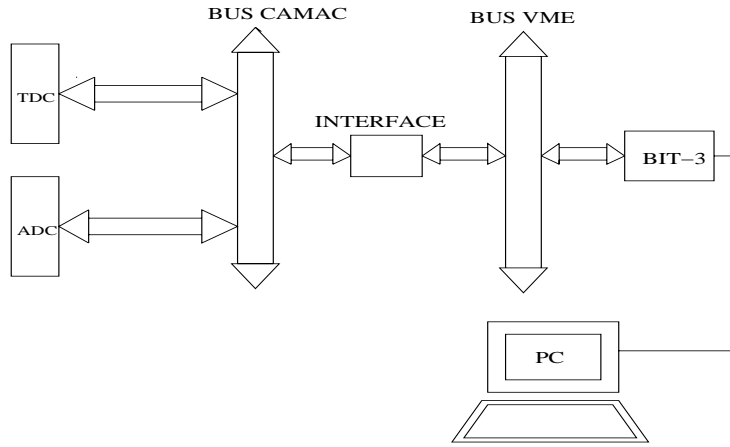


Figure 7: Scheme of the readout of TDC and ADC signals.

4.1 Detection efficiency

Detection efficiencies of the PMT's were measured as $\epsilon = \frac{N_{PMT}}{N_T}$, where N_T is the number of cosmic rays selected by a telescope and N_{PMT} is the corresponding number for each PMT of the counter under test. The high voltage for each counter was chosen to maximize ϵ while keeping the count frequency due to thermal noise of the PMT's within reasonable values. Initial values V_0 for the PMT high voltage were set about 50 V beyond the knee of the efficiency curve for events crossing the telescope that was at the opposite edge from the PMT (see fig.8). Data at three different HV values $V > V_0$ were collected in this way. For $V > V_0$ the counters' efficiency did not depart from the maximum value $\epsilon = 1$ within $N_T \simeq 500$ counts.

4.2 Time resolution: a first evaluation

When a particle crosses a scintillator at distance x from its center at the time t_0 , the time differences Δt_L , Δt_R between signals of the Left and Right PMT's and the signal t_s of telescope placed in x are given by [5]:

$$\Delta t_{L,R} = t_0 + \frac{l/2 \pm x}{v_{eff}} - t_s \quad (1)$$

where l is the length of the scintillator and v_{eff} is the effective light speed inside it. For the scintillators under test,

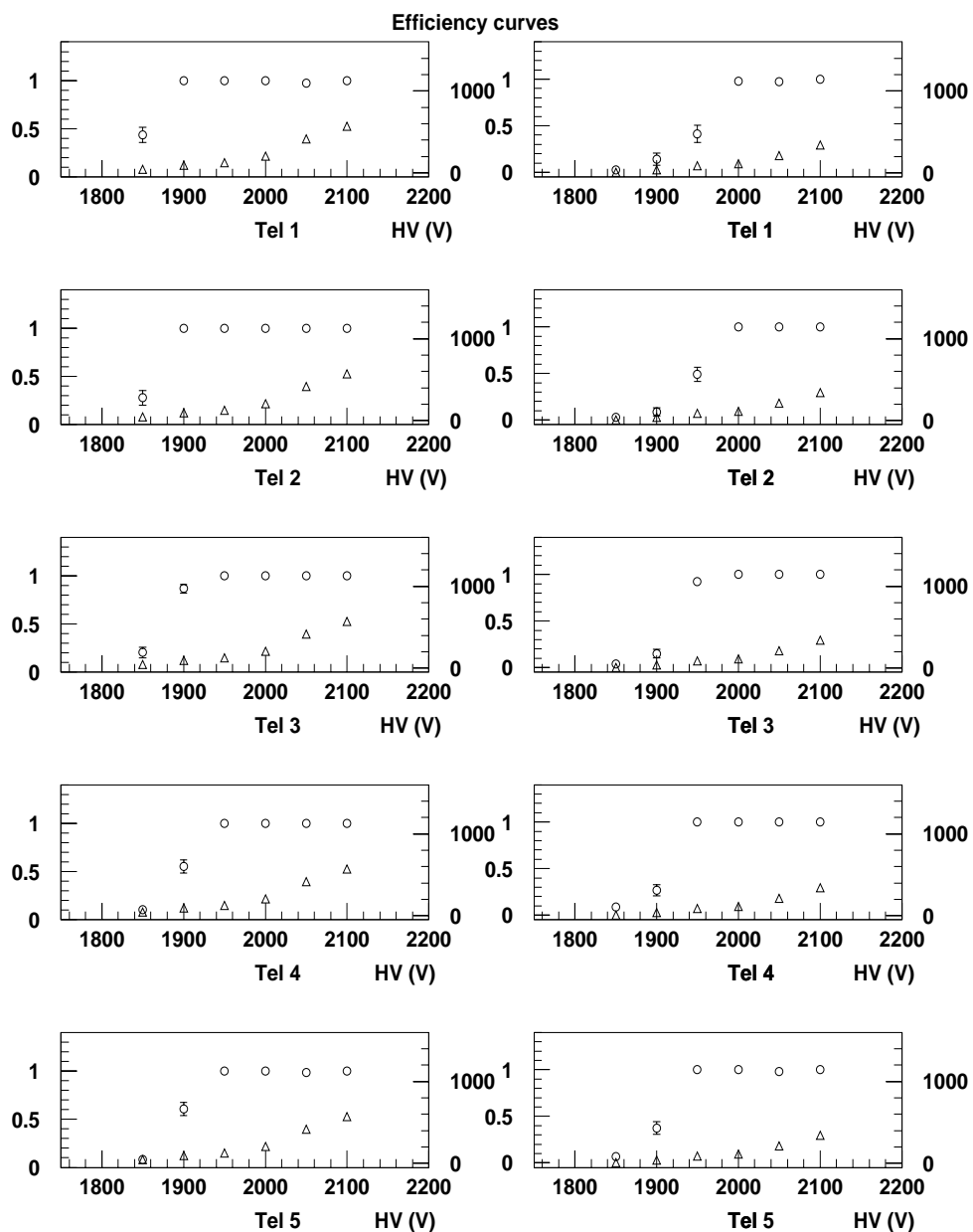


Figure 8: Detection efficiencies (\circ , left scale [%]) and noise count frequencies (Δ , right scale [Hz]) as a function of the high voltage V , for counter n. 56 of TOF-WALL. The two columns refer to the two PMT's of the counter.

$$v_{eff}^{-1} \sim 5.9 \text{ ns/m}. \quad (2)$$

The quantity:

$$\Delta t_+ = \frac{\Delta t_L + \Delta t_R}{2} = t_0 + \frac{l}{2v_{eff}} - t_s \quad (3)$$

is independent of x and allows the measurement of the time of flight, while the time difference:

$$\Delta t_- = \frac{\Delta t_L - \Delta t_R}{2} = \frac{x}{v_{eff}} \quad (4)$$

allows to reconstruct the x position of the event along the counter.

The intrinsic resolutions of PMT's $\sigma_{t_{L,R}}$ can be obtained from the time distributions measured in the test:

$$\sigma_{t_{L,R}}^2 = \sigma_{\Delta t_{L,R}}^2 - \sigma_s^2 \quad (5)$$

where $\sigma_{\Delta t_{L,R}}$ are the corresponding resolutions from a gaussian fit of the distributions of times $\Delta t_{L,R}$ (see fig.9), and σ_s is the cosmic ray telescope time resolution, which can be evaluated from the resolutions $\sigma_{\Delta t_+}$ and $\sigma_{\Delta t_-}$ as:

$$\sigma_s^2 = \sigma_{\Delta t_+}^2 - \sigma_{\Delta t_-}^2, \quad (6)$$

where the double contribution from the start signal in Δt_+ cancels in Δt_- . It follows that the intrinsic time resolution:

$$\sigma_C = \frac{1}{2} \sqrt{\sigma_{t_L}^2 + \sigma_{t_R}^2} \quad (7)$$

is expected to be equivalent to the one calculated directly from the distribution of events $\frac{1}{2}(\Delta t_L - \Delta t_R)$. As already observed for eq. (4), the finite size of the telescopes introduces a geometrical contribution σ_G to $\sigma_{\Delta t_-}$:

$$\sigma_G = \frac{\Delta x}{v_{eff} \sqrt{12}} \quad (8)$$

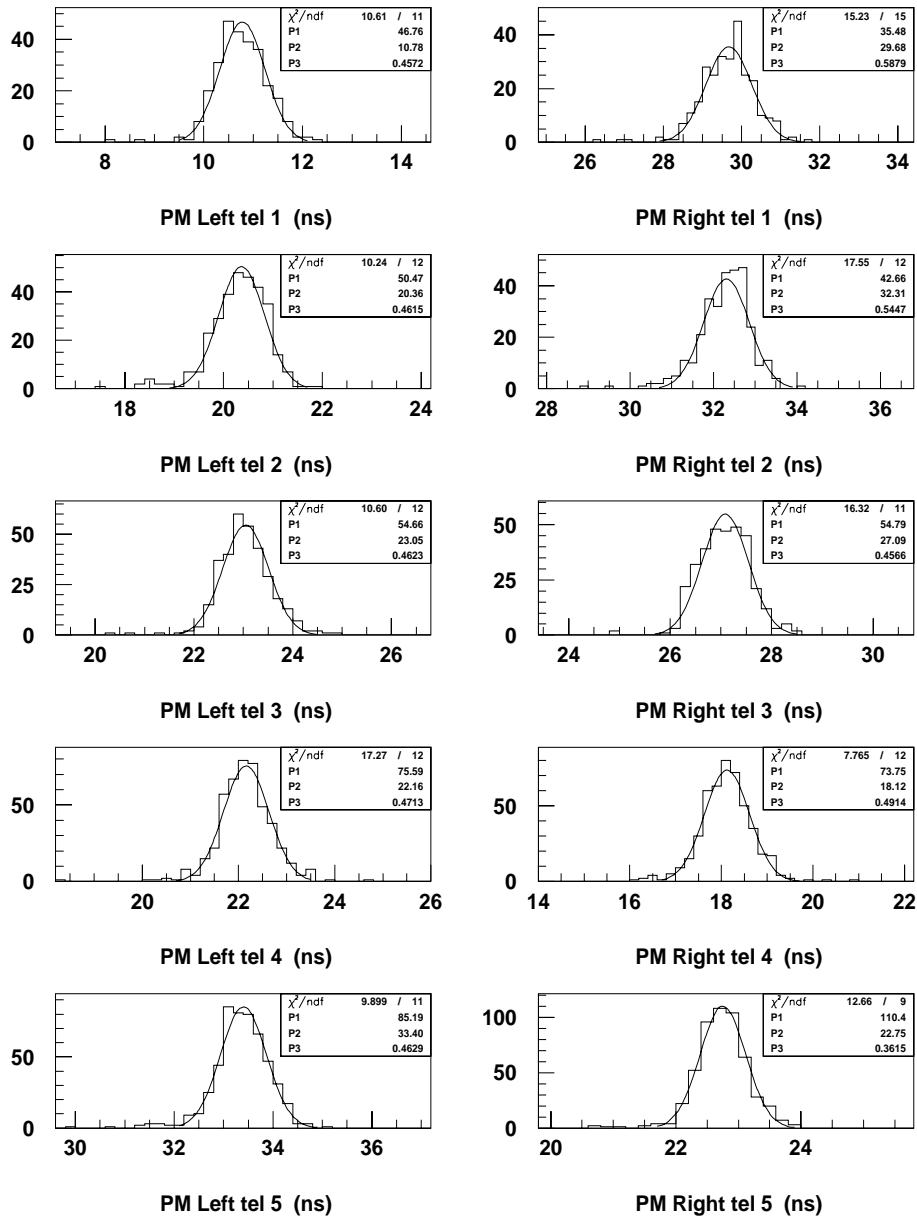


Figure 9: Measured time distributions in the Left and Right PMT's of counter 13, for events triggered by the five telescope counters.

Table 1: Mean values of σ_s for the five telescopes.

Tel	σ_s (ns)
1	0.393
2	0.366
3	0.389
4	0.367
5	0.289

Therefore the effective resolution $\sigma_{\Delta t_-}^{eff}$ can be estimated as (see eq. (2)):

$$\sigma_{\Delta t_-}^{eff\ 2} = \sigma_{\Delta t_-}^2 - 2.9 \cdot (\Delta x)^2, \quad (9)$$

and the correct values of σ_s for the telescopes are:

$$\sigma_s^{eff\ 2}(i) = \sigma_{\Delta t_+}^2 - \sigma_{\Delta t_-}^2 + 2.9 \cdot (\Delta x)^2(i), \quad i = 1, \dots, 5. \quad (10)$$

The working voltage for each PMT was determined from the three sets of data recorded with different V values, optimizing the value of $\sigma_{\Delta t_-}$ while keeping the noise rate acceptable.

The values of σ_s for the five telescopes were then calculated. Their mean values (see tab.1) were used to estimate the intrinsic resolutions of the PMT's σ_{t_L} and σ_{t_R} (5), and σ_C (7), and the corresponding average values for each position along the counters (see tab. 2). The resolutions averaged over the five selected positions were found to be:

$$\sigma_C(L = 250cm) = (208 \pm 15)ps \quad (11)$$

$$\sigma_C(L = 180cm) = (201 \pm 15)ps. \quad (12)$$

The intrinsic PMT time resolution with the closer telescope was systematically better than the one measured at 170 cm or 240 cm from the same PMT (see fig.10). This reflects the dependence of the resolution on photostatistics and on the photon time spread at the photocatode. As a consequence, the determination of the crossing time t_0 with the simple arithmetic mean (3) can be improved.

Table 2: Average resolutions σ_{t_L} , σ_{t_R} and σ_C and corresponding *rms* values of counters $L = 250$ cm and $L = 180$ cm at the different telescope positions (see fig.4 for the geometry).

$L = 250$ cm, 26 counters				$L = 180$ cm, 13 counters			
Tel	σ_{t_L} (ps)	σ_{t_R} (ps)	σ_C (ps)	Tel	σ_{t_L} (ps)	σ_{t_R} (ps)	σ_C (ps)
1	169 ± 64	352 ± 73	203 ± 36	1	176 ± 37	321 ± 36	199 ± 20
2	250 ± 64	339 ± 42	212 ± 30	2	255 ± 53	248 ± 37	219 ± 69
3	241 ± 61	277 ± 63	177 ± 40	3	268 ± 40	282 ± 44	189 ± 22
4	296 ± 38	278 ± 63	204 ± 25	4	252 ± 40	241 ± 61	184 ± 21
5	367 ± 63	291 ± 66	243 ± 35	5	341 ± 73	251 ± 61	214 ± 35

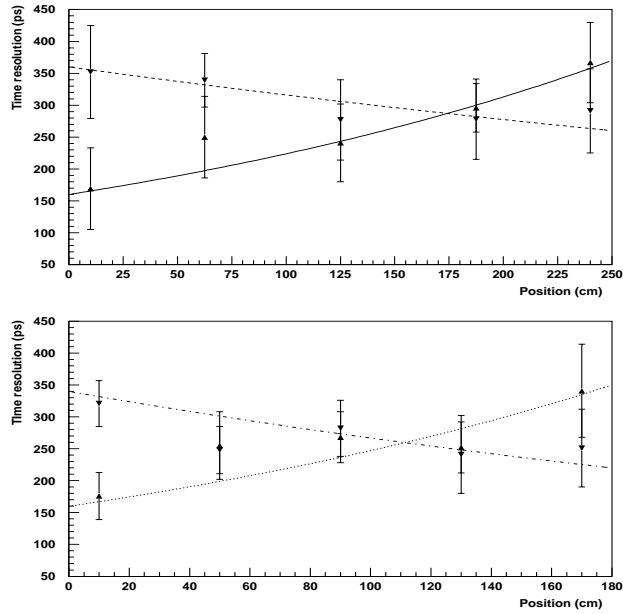


Figure 10: Average resolutions σ_{t_L} (\blacktriangle) and σ_{t_R} (\blacktriangledown) as a function of the distance from the the Left PMT, along $L = 250$ cm (above) and $L = 180$ cm (below) counters (the centers of the counters are at 125 cm and at 90 cm respectively). The error bars show the *rms* of the distributions. The curves are meant to guide the eye.

If the position x of the hit along the counter can be measured independently from time with better resolution (as it will be in HARP, using the tracking system) it will be possible to obtain a crossing time measurement with a better precision than eq. (3). In this new approach it is possible to correct the times for the position:

$$\Theta_L = t_L - \frac{l/2 - x}{v_{eff}} \quad (13)$$

$$\Theta_R = t_R - \frac{l/2 + x}{v_{eff}} \quad (14)$$

and to build a likelihood function $\mathcal{L}(\Theta_L, \Theta_R, t_0) = N e^{-\frac{(\Theta_L - t_0)^2}{2\sigma_{t_L}^2}} e^{-\frac{(\Theta_R - t_0)^2}{2\sigma_{t_R}^2}}$ taking into account the different time resolutions σ_{t_L} and σ_{t_R} along the counters (N is a normalization factor).

Maximizing the \mathcal{L} value for the crossing time t_0 and neglecting the error on x , a weighted intrinsic resolution is found:

$$\frac{\partial \log(\mathcal{L})}{\partial t_0} = 0 \implies t_0^W = \frac{t_L \sigma_{t_R}^2 + t_R \sigma_{t_L}^2}{\sigma_{t_L}^2 + \sigma_{t_R}^2} - \frac{l}{2v_{eff}} - \frac{x}{v_{eff}} \frac{\sigma_{t_L}^2 - \sigma_{t_R}^2}{\sigma_{t_L}^2 + \sigma_{t_R}^2}; \quad (15)$$

$$\sigma_{t_0} = \sigma_C^W = \sqrt{\left[\frac{1}{\sigma_{t_L}^2} + \frac{1}{\sigma_{t_R}^2} \right]^{-1}}. \quad (16)$$

The intrinsic resolution of this method σ_C^W (see eq. (16)) is close to σ_C (see eq. (7)) at the center of the counter ($x = 0$), but is certainly better than σ_C at the ends of the scintillator (see fig.11 and tab.3), where the resolution is dominated by the near PMT.

The averages of σ_C^W over the five positions are now (cfr. eq. (11) and (12)):

$$\sigma_C^W(L = 250cm) = (197 \pm 18)ps \quad (17)$$

$$\sigma_C^W(L = 180cm) = (185 \pm 18)ps. \quad (18)$$

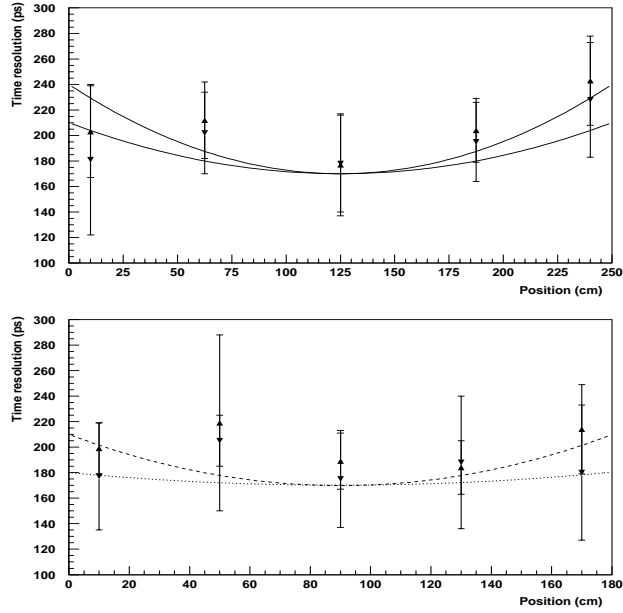


Figure 11: Time resolutions obtained from (16) (\blacktriangledown) and (7) (\blacktriangle) as a function of the position as evaluated starting from PMT Left, along the counters with $L = 250$ cm (above) and $L = 180$ cm (below) (the centers of the counters are at 125 cm and at 90 cm respectively). The error bars show the *rms* of the distributions. The curves are meant to guide the eye.

Table 3: The average intrinsic counter resolutions and *rms* values obtained with the likelihood method (to be compared with table 2).

$L = 250$ cm, 26 counters		$L = 180$ cm, 13 counters	
Tel	σ_C^W (ps)	Tel	σ_C^W (ps)
1	181 ± 59	1	177 ± 42
2	202 ± 32	2	205 ± 20
3	178 ± 38	3	175 ± 38
4	195 ± 31	4	188 ± 52
5	228 ± 45	5	180 ± 53

4.3 Analysis of charge spectra

PMT charge spectra show a characteristic asymmetric tail at large values (see fig.12). Spectra were fitted to a Landau distribution:

$$f(Q) = N e^{-\frac{1}{2}(2.22 \frac{Q-Q_{pk}}{\sigma} + e^{-2.22 \frac{Q-Q_{pk}}{\sigma}})} \quad (19)$$

providing three fit parameters N , Q_{pk} and σ : Q_{pk} corresponds to the peak position, σ measures the width and N is a normalization factor. Owing to the light attenuation along the scintillator, the charge collected by a phototube decreases, as expected, with the distance l from the particle's impact point (see fig.13):

$$Q(l) = Q_0 e^{-\frac{l}{\lambda}}, \quad (20)$$

where λ is the characteristic attenuation length.

Figure 13 also shows a saturation of the signal close to the PMT's. This can result from two opposite competing effects: the increase in the number of the direct photons due to the increase of the solid angle covered by the photocathode and the reduction of the signal due to back reflections by the light guide, more probable for positions closer to the PMT. The measurement with the telescope close to the PMT was therefore discarded in the attenuation length fit procedure to avoid biases. The estimates of λ with the Right and Left PMT are compatible (within uncertainties). For the long and the short counters the average and *rms* are (see fig.14):

$$\lambda(L = 250cm) = (414 \pm 42)cm \quad (21)$$

$$\lambda(L = 180cm) = (349 \pm 41)cm \quad (22)$$

from which the overall result (see fig.15) is:

$$\lambda = 395 \pm 51 cm. \quad (23)$$

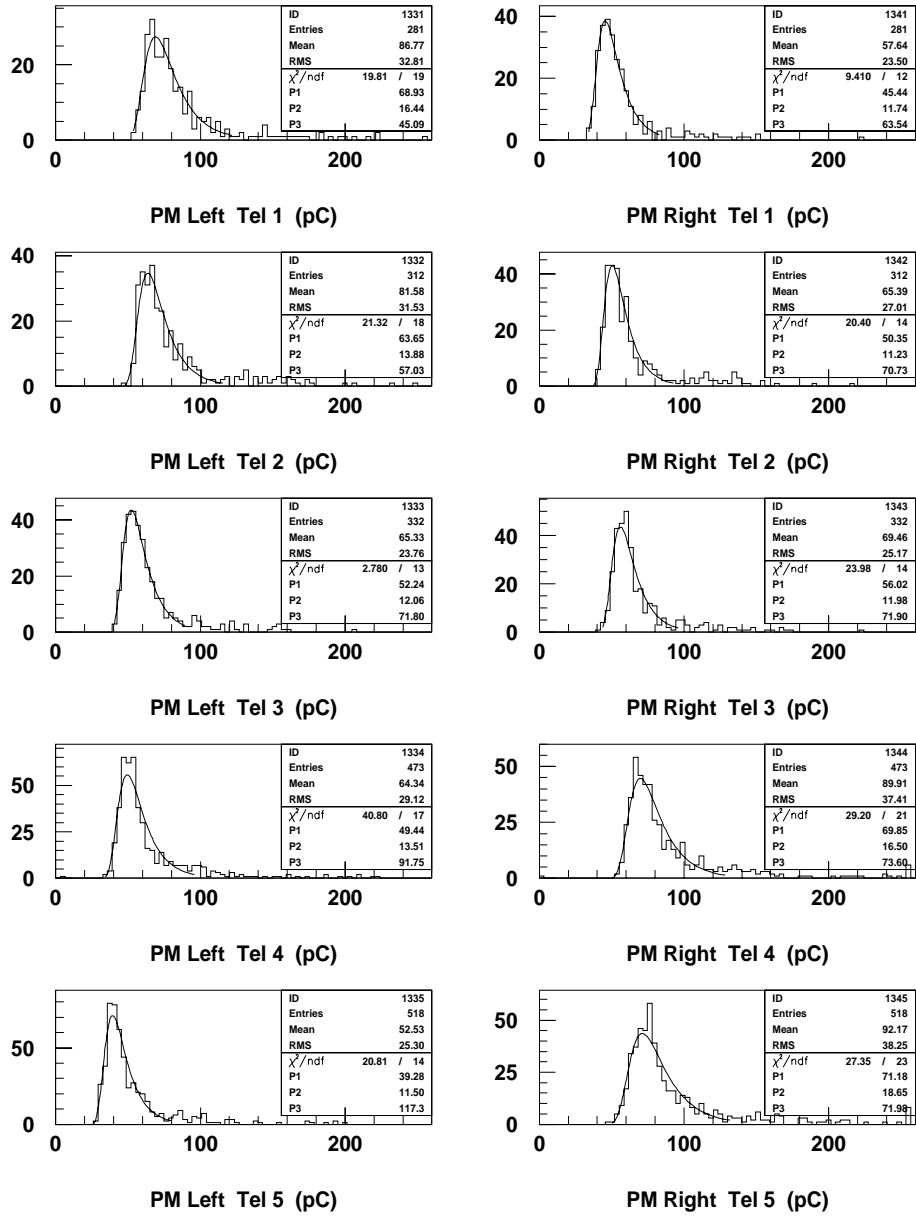


Figure 12: Charge spectra and Landau fit for the counter 13 of TOF-WALL.

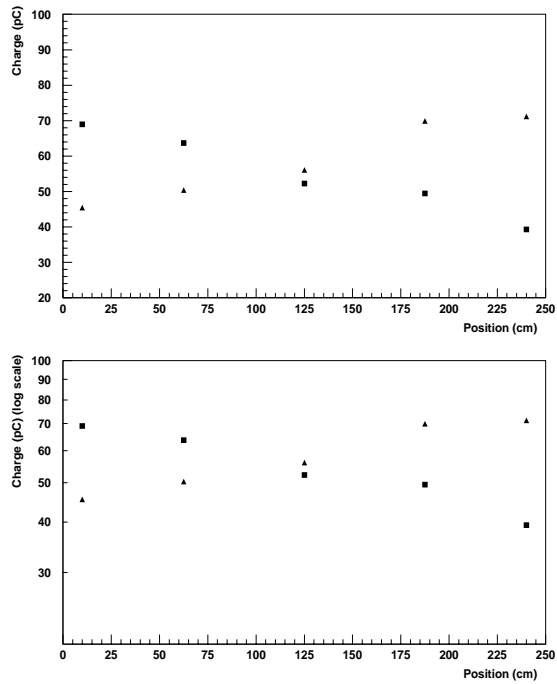


Figure 13: Values of the charge as a function of the position along the counter n. 13 of the TOF-WALL. ■ = Left PMT; ▲ = Right PMT.

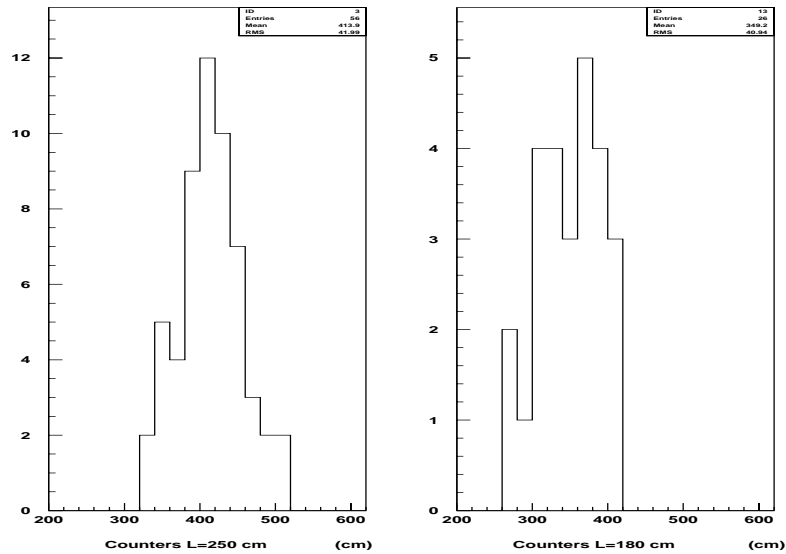


Figure 14: Distributions of the attenuation lengths measured in the counters $L = 250$ cm and $L = 180$ cm.

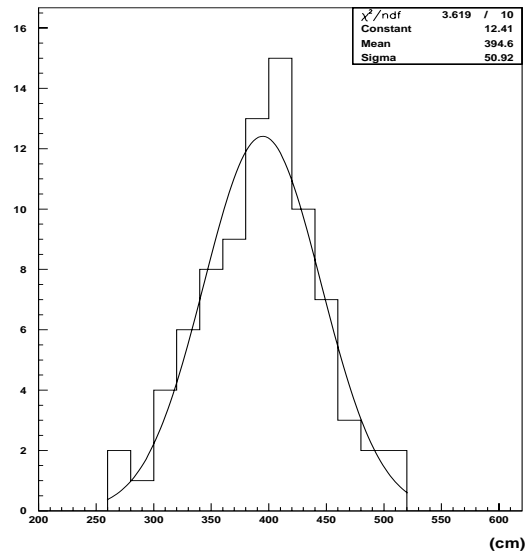


Figure 15: Distribution of the attenuation lengths measured in all the HARP TOF-WALL counters.

4.4 Time resolution: time walk correction

The adoption of leading edge discriminators introduces a dependence of the discrimination times on the collected charge (*time walk*) as shown in fig.16, which affects the intrinsic time resolution. A second contribution to time walk is due to the sensitivity of the real discriminator to the charge: when the threshold is crossed, a finite amount of charge is needed to turn the discriminator on (dashed triangles in fig.16), and the time delay to collect it is larger for small pulses.

To take these effects into account, correction terms $\delta t_{L,R}$ to the measured times $\Delta t_{L,R}$ were determined as a function of the corresponding charge signal. These corrections are usually parameterized by the formula [6]:

$$\delta t = W \left(\frac{1}{\sqrt{A_0}} - \frac{1}{\sqrt{A}} \right) \quad (24)$$

where A is the associated charge, A_0 is a reference charge and W is the walk parameter, to be determined experimentally. For this purpose, the time t was plotted for every PMT as a function of charge A and of $A^{-1/2}$, gathering together the data relative to all the five telescopes. After the equalization of the average times (the times recorded with the first four telescopes were shifted to have the same average time as the telescope five, taken as a reference), a continuous curve is obtained for t as a function of A . Moreover,

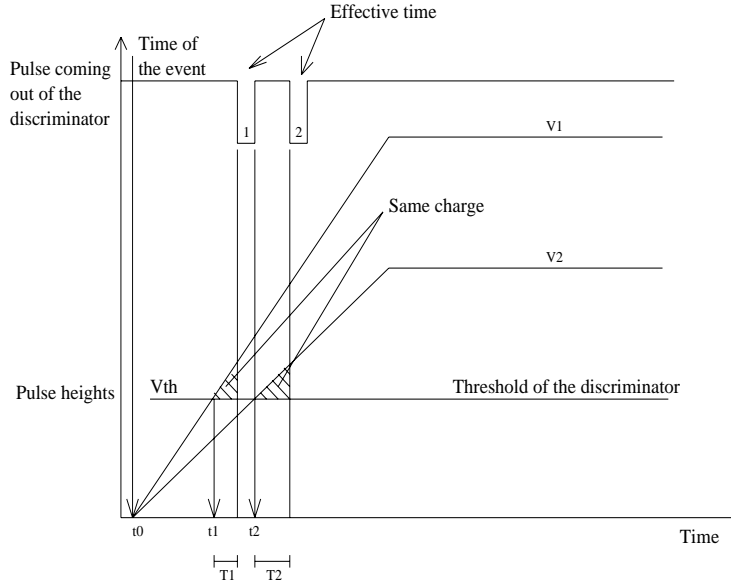


Figure 16: Sketch showing the time walk t_1 , t_2 and delays T_1 , T_2 to turn on the discriminator for two different signal amplitudes V_1 and V_2 .

a correction was applied because the mean values of the time distributions of the five telescopes do not correspond to the same value of charge: from the plot of t as a function of A , relative only to the telescope number five (see fig.17), the corrections Δt relative to the other four telescopes were obtained. Times t were averaged for fixed values of A and $A^{-1/2}$ inside bins of appropriate width (5 pC and $0.0125 \text{ pC}^{-1/2}$, respectively). As expected, (see fig.18):

- the values of the measured times decreased with the increasing of the charge;
- the dependence of t as a function of $A^{-1/2}$ was roughly linear.

The distribution of W measured at the Left PMT is quite similar to the corresponding one for the Right PMT (see fig.19): the average value is $\sim 11.4 \text{ ns} \cdot \text{pC}^{1/2}$. A_0 was fixed to the mean values of the charge distributions. The corrections $\delta t_{L,R}$ obtained in this way were included event by event in the $\Delta t_{L,R}$ determination:

$$(\Delta t_L)_C = \Delta t_L + \delta t_L = (t_L - t_s) + \delta t_L = (t_L)_C - t_s \quad (25)$$

$$(\Delta t_R)_C = \Delta t_R + \delta t_R = (t_R - t_s) + \delta t_R = (t_R)_C - t_s. \quad (26)$$

Figure 20 shows that the distributions of the times after the correction are on average narrower than those before correction (see fig.9) but the mean values of such distributions are

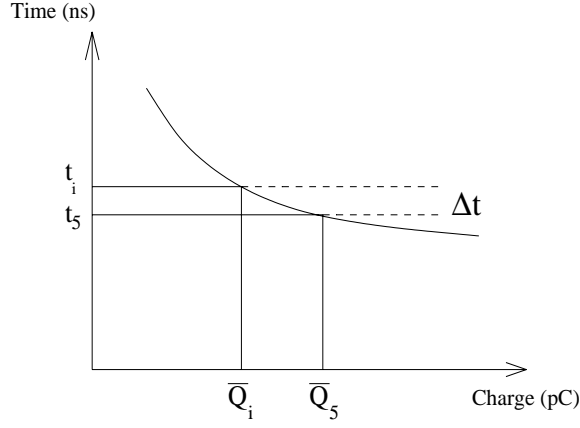


Figure 17: Δt contribution to the distributions of t as a function of A .

not modified in a significant way. Intrinsic resolutions were then recalculated correcting for the contribution of the start of the telescopes (see tab.4), obtaining, on average, an improvement in intrinsic resolution of about 40 ps (49 ps) for the counters of length $L = 250$ cm ($L = 180$ cm). After this last corrections the resolutions averaged over the five telescopes for the two counter lengths are:

$$\sigma_C(L = 250 \text{ cm}) = (168 \pm 17) \text{ ps} \quad (27)$$

$$\sigma_C(L = 180 \text{ cm}) = (152 \pm 12) \text{ ps}. \quad (28)$$

The procedure of correction of the time walk effect described above improves of the resolutions of the counters with respect to the values estimated in 4.2. However it has to be noticed that in the calculation in 4.2 of the intrinsic PMT time resolution $\sigma_{t_{L,R}}^2 = \sigma_{\Delta t_{L,R}}^2 - \sigma_s^2$ the time walk effect was partially included because of the evaluation of σ_s from $\sigma_{\Delta t_+}$, $\sigma_{\Delta t_-}$. As a consequence, the improvement of the resolution due to this correction would be larger than what deducible from the comparison between (11)-(12) and (27)-(28). If the procedure for the calculation of σ_C^W by the likelihood function \mathcal{L} is repeated, an average improvement in resolution of 32 ps (40 ps) for $L = 250$ cm ($L = 180$ cm) (see table 5 and figure 21) is obtained:

$$\sigma_C^W(L = 250 \text{ cm}) = (165 \pm 15) \text{ ps} \quad (29)$$

$$\sigma_C^W(L = 180 \text{ cm}) = (145 \pm 14) \text{ ps}. \quad (30)$$

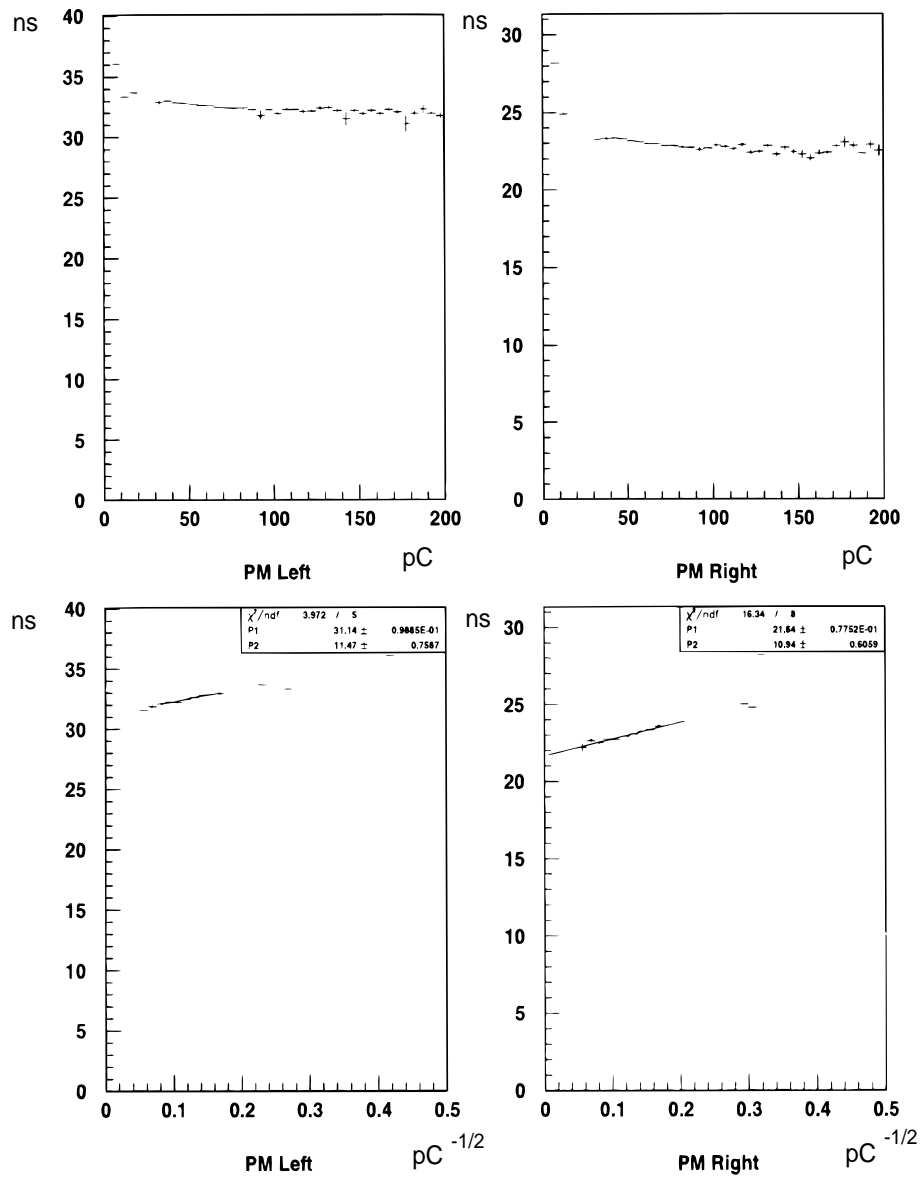


Figure 18: Dependence of time on charge, counter 38, Left and Right PMT.

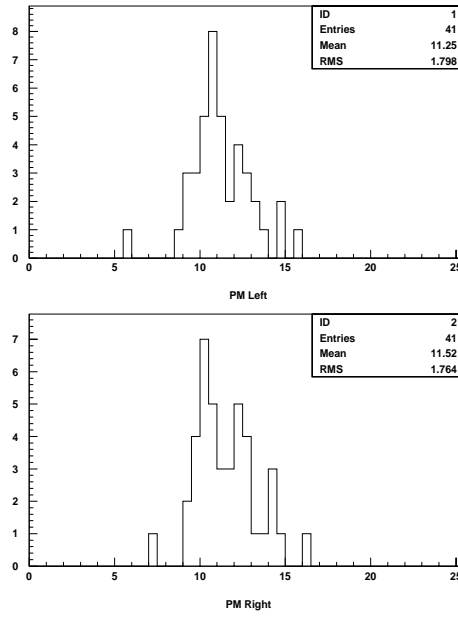


Figure 19: Distributions of the time walk parameter W ($\text{ns} \cdot \text{pC}^{1/2}$) for Left and Right PMT's.

Table 4: Average resolutions corrected for time walk and *rms*.

$L = 250$ cm, 26 counters				$L = 180$ cm, 13 counters			
Tel	σ_{t_L} (ps)	σ_{t_R} (ps)	σ_C (ps)	Tel	σ_{t_L} (ps)	σ_{t_R} (ps)	σ_C (ps)
1	170 ± 58	302 ± 10	167 ± 49	1	122 ± 49	318 ± 39	168 ± 18
2	208 ± 71	292 ± 58	178 ± 37	2	220 ± 25	198 ± 35	150 ± 27
3	190 ± 71	245 ± 73	149 ± 35	3	200 ± 38	222 ± 40	140 ± 19
4	220 ± 52	217 ± 58	164 ± 34	4	215 ± 26	180 ± 21	142 ± 40
5	294 ± 42	208 ± 56	184 ± 35	5	256 ± 30	179 ± 49	158 ± 28

Table 5: Average time walk corrected (\pm *rms*) intrinsic resolutions as calculated with the likelihood method.

$L = 250$ cm, 26 counters		$L = 180$ cm, 13 counters	
Tel	σ_C^W (ps)	Tel	σ_C^W (ps)
1	174 ± 10	1	154 ± 19
2	166 ± 49	2	145 ± 44
3	142 ± 38	3	130 ± 28
4	158 ± 30	4	142 ± 40
5	183 ± 44	5	153 ± 27

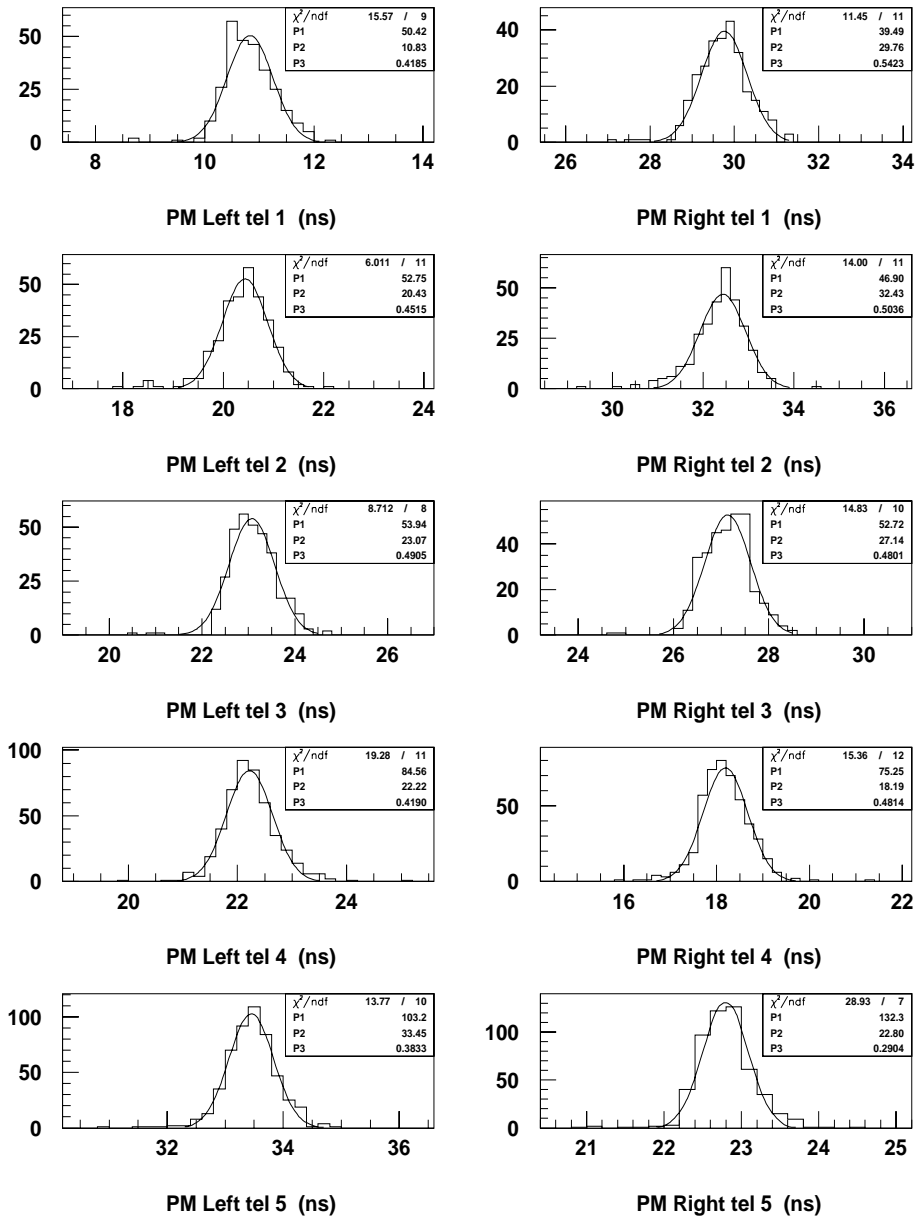


Figure 20: Time distributions, corrected for the time walk, for the Left and Right PMT's of TOF-WALL counter n. 13 (for the uncorrected distributions see fig.9).

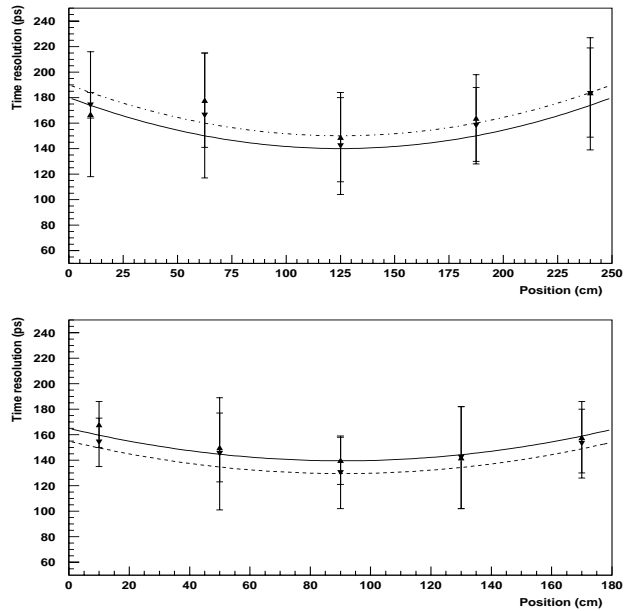


Figure 21: Time resolutions as obtained by (16) (\blacktriangledown) and by (7) (\blacktriangle) as a function of the distance from the Left PMT, along the counters with $L = 250$ cm (above) and $L = 180$ cm (below) (the centers of the counters are at 125 cm and at 90 cm respectively). The error bars show the *rms* of the distributions.

5 Conclusions

The analysis of the performances of the scintillator counters used for the TOF-WALL detector of the HARP experiment showed that:

1. all counters are fully efficient ($\epsilon = 1$ within statistics), with low (< 1 KHz) single counting rate: the scintillators are therefore able to detect all the secondary particles expected to hit the TOF-WALL;
2. the attenuation length λ of the scintillation light inside the counters is about 400 cm, therefore a large fraction of the photons reaches the PMT's photocatode (maximum distance 250 cm);
3. the intrinsic resolution σ_C of the counters on the crossing time of a particle, determined as $t_0 = \frac{t_L + t_R}{2}$, is on average 208 ps (201 ps) for $L = 250$ cm ($L = 180$ cm);
4. in HARP the resolution on the crossing time can be improved by the knowledge of the particle's impact point along the counter (measured by drift chambers). In this case σ_C^W reaches 197 ps (185 ps) for $L = 250$ cm ($L = 180$ cm);
5. by correcting the measured times for the PMT signal amplitude dependence (time walk) the time resolutions improve to $\sigma_C^W = 165$ ps (145 ps) for $L = 250$ cm ($L = 180$ cm);
6. the resolution of the short counters ($L = 180$ cm) is better than that of the long counters ($L = 250$ cm), therefore the former are more suitable for the central part of the TOF-WALL, where the most energetic particles produced at the HARP target are expected.

Acknowledgements

We are greatly indebted to F. Chignoli of INFN Milano, D. Filippi, P. Gesuato, D. Mazzaro and M. Turcato of INFN Padova for technical help in the preparation and test of the counters.

References

- [1] M.G. Catanesi et al.: CERN-SPSC/99-35, SPSC/P315, 1999.
- [2] www.bicron.com for data on BC-408 by Bicron.
- [3] Philips data handbook for data on PM XP2020.
- [4] M. Bonesini et al., "*Construction of a fast laser-based calibration system for the Harp Tof counter wall*", submitted to IEEE 2002, Norfolk.
- [5] M.Baldo Ceolin et al., Nuovo Cim. **105A**, 1679-1692 (1992).
- [6] W.Braunschweig et al., Nucl. Instr. and Meth. **134**, 261-266 (1976).